Reconstructing the primary reflections in seismic data by Marchenko redatuming and convolutional interferometry

Meles, Giovanni; Wapenaar, Kees; Curtis, A

Important note
To cite this publication, please use the final published version (if applicable).
Please check the document version above.

Reconstructing the primary reflections in seismic data by Marchenko redatuming and convolutional interferometry

Giovanni Angelo Meles[1], Kees Wapenaar[2], and Andrew Curtis[1]

ABSTRACT

State-of-the-art methods to image the earth's subsurface using active-source seismic reflection data involve reverse time migration. This and other standard seismic processing methods such as velocity analysis provide best results only when all waves in the data set are primaries (waves reflected only once). A variety of methods are therefore deployed as processing to predict and remove multiples (waves reflected several times); however, accurate removal of those predicted multiples from the recorded data using adaptive subtraction techniques proves challenging, even in cases in which they can be predicted with reasonable accuracy. We present a new, alternative strategy to construct a parallel data set consisting only of primaries, which is calculated directly from recorded data. This obviates the need for multiple prediction and removal methods. Primaries are constructed by using convolutional interferometry to combine the first-arriving events of upgoing and direct-wave downgoing Green's functions to virtual receivers in the subsurface. The required upgoing wavefields to virtual receivers are constructed by Marchenko redatuming. Crucially, this is possible without detailed models of the earth's subsurface reflectivity structure: Similar to the most migration techniques, the method only requires surface reflection data and estimates of direct (nonreflected) arrivals between the virtual subsurface sources and the acquisition surface. We evaluate the method on a stratified synclinal model. It is shown to be particularly robust against errors in the reference velocity model used and to improve the migrated images substantially.

INTRODUCTION

Although advanced methods of seismic data processing such as recursive imaging (Malcolm et al., 2009) or full-waveform inversion (Virieux and Operto, 2009) can properly take into account data that include multiply scattered waves, many current standard processing steps are based on the so-called Born approximation. This approximation assumes that waves have only scattered from heterogeneities in the medium once, thus requiring that data consist only of primaries — singly scattered waves. These processing steps include normal moveout correction and velocity analysis (Yilmaz, 2001) and imaging reflectors using standard linear migration (Zhu et al., 1998; Gray et al., 2001). Multiples represent a source of coherent noise for such methods and must be suppressed to avoid artifacts.

Multiples related to reflections from the earth's free surface particularly impact on images resulting from seismic marine data, and much effort has been devoted to their removal (see the review by Dragoset et al., 2010). In contrast, internal multiples affect both marine and land data, and relatively fewer techniques exist to predict and remove them from reflection data. Berkhout and Verschuur (1997) iteratively extrapolate shot records to successive reflecting boundaries responsible for multiple generation. Jakubowicz (1998) uses combinations of three observed reflections to predict and remove multiples, which led to several other variations on that theme (Behura and Forghani, 2012; Hung and Wang, 2012). However, the above schemes require significant prior information about subsurface reflectors or reflections prior to multiple prediction and removal. Inverse scattering methods for multiple prediction (Weglein et al., 1997, 2003) do not demand so much information but tend to be computationally expensive (Wang et al., 2012). Meles et al. (2015) propose an internal multiple prediction method based on a combined use of seismic interferometry and Marchenko redatuming.

Seismic interferometry techniques synthesize Green's functions between source (or receiver) locations by integrating crosscorrelations or convolutions of wavefields recorded by receivers (or emanating from sources) located elsewhere (Campillo and Paul, 2003;

Wapenaar, 2004; van Manen et al., 2005, 2006; Wapenaar and Fokkema, 2006). With these methods, one of the sources (or receivers) is basically turned into a virtual receiver (or source).

Marchenko redatuming estimates up- and downgoing components of Green's functions between an arbitrary location inside a medium such as the earth's subsurface in which no sources (or receivers) are placed, and real receivers (or sources) located at the surface (Broggini et al., 2012; Wapenaar et al., 2012, 2014a; da Costa Filho et al., 2014; Wapenaar, 2014). In contrast to interferometry but similarly to standard linear migration methods, Marchenko redatuming requires an estimate of the direct wave from the virtual source (or to the virtual receiver), illumination from only one side of the medium, and no physical sources (or receivers) inside the medium.

In principle, redatumed Green's functions can be used to provide multiple-free images directly (Behura et al., 2014; Broggini et al., 2014; da Costa Filho et al., 2015; van der Neut et al., 2015). However, this approach requires as many virtual sources as there are image points in the subsurface and many correlation or deconvolution operations. It is thus computationally feasible only if we wish to image a small portion of the subsurface. Marchenko redatuming also allows one to perform redatuming of surface reflectivity to a finite number of depth levels and to apply standard imaging in between those datum levels (Wapenaar et al., 2014b; Ravasi et al., 2016). In that case, however, the redatumed reflectivities include internal multiples reverberating below the redatuming level, which again may diminish the quality of resulting images if they are not removed prior to imaging.

Using an approach similar to that used by Meles et al. (2015) to predict multiples, we propose a new method to estimate primaries directly based on convolutional interferometry and Marchenko redatuming. This obviates the need to subtract multiples from recorded data, and it produces a primaries-only data set that can be imaged without multiple-related artifacts using standard methods of linear migration. We demonstrate the method on a synthetic data set and show that it is particularly robust against errors in initial estimates of the velocity structure.
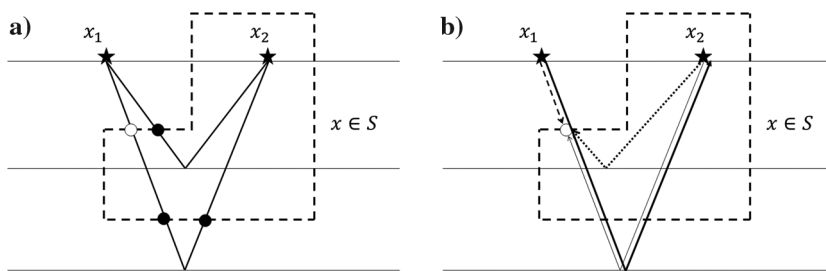
METHODS

Convolutional interferometry uses acoustic reciprocity theorems to express the Green's function between two locations as follows (van Manen et al., 2005):

$$G(x_2, x_1) = \int_S \frac{1}{\rho(x)} \{ G(x, x_2) n_i \partial_i G(x, x_1) $$
$$- n_i \partial_i G(x, x_2) G(x, x_1) \} dS. \quad (1)$$

Here, $\rho(x)$ denotes density, x_1 and x_2 are two source (or receiver) positions, $G(x_2, x_1)$ represents the frequency-domain Green's function recorded at x_2 for an impulsive volume injection rate source at x_1, S is an arbitrary boundary of receivers (sources) enclosing either x_1 or x_2 but not both (Figure 1a), and n_i and ∂_i represent the ith Cartesian component of the normal vector to S, and of the gradient, respectively. Einstein summation applies over repeated indices, and we have applied source-receiver reciprocity to the expressions in van Manen et al. (2005).

We can approximate equation 1 using a one-way wave propagation formalism and by approximating dipoles (derivatives) as follows (Wapenaar and Berkhout, 1989; Wapenaar and Fokkema, 2006; Wapenaar et al., 2011):

$$G(x_2, x_1) \approx \int_S \frac{2j\omega}{c(x)\rho(x)} \{ G^-(x, x_2) G^+(x, x_1) $$
$$- G^+(x, x_2) G^-(x, x_1) \} dS, \quad (2)$$

where $c(x)$ indicates wave speed, and $G^{+/-}$ represents down/upgoing Green's function components at the boundary S. The main contributions to the evaluation of such interferometric surface integrals come from neighborhoods of points at which the phase of the integrand is stationary (Snieder et al., 2006), and some example stationary points for the reflected waves are indicated by circles in Figure 1a.

For the geometries considered here, these stationary points are located inside the medium, and usually the corresponding Green's functions in the integrand ($G^{+/-}(x, x_1)$ and $G^{+/-}(x, x_2)$) can be neither directly measured nor modeled accurately because this would require either the presence of receivers in the subsurface or knowledge of the exact subsurface velocity and density distributions. However, Marchenko redatuming provides estimates of all such Green's functions from surface sources at x_1 or x_2 to receivers located in the subsurface at points x (Figure 1a), given only surface reflection data and an estimate of the direct (nonreflected) wavefield from the surface to x (Broggini et al., 2012; Wapenaar et al., 2012, 2014a).

Figure 1a illustrates how primary reflections are reconstructed in convolutional interferometry: Equations 1 and 2 essentially piece together and integrate wavefields traveling upward and downward from around each stationary point to calculate wavefields that would travel along each full wavepath between x_1 and x_2. Meles

Figure 1. Geometric configurations that construct primaries from convolutional interferometry. The stars are sources at x_1 and x_2, and the dashed lines indicate ideal receiver boundaries S. (a) The circles indicate stationary points associated with primary reflections between x_1 and x_2. At each such point, convolutional interferometry connects direct and the first-order scattering events to create the primary waves between x_1 and x_2. The filled circles indicate stationary points x connecting direct waves $G_D^+(x, x_1)$ and the first-arriving reflection in $G^-(x, x_2)$ or $G_D^+(x, x_2)$ and the first-arriving reflection in $G^-(x, x_1)$. The unfilled circle indicates a stationary point x not connecting $G_D^+(x, x_1)$ and the first-arriving reflection in $G^-(x_2, x)$. This is better illustrated in (b): the primary reflection event $G(x_2, x_1)$ indicated by the thick ray is constructed by joining an upgoing scattered event in $G^-(x, x_2)$ and a direct wave $G_D^+(x, x_1)$ (thin solid and dashed rays, respectively). In this case, the first-arriving event of $G^-(x, x_2)$ is a reflection coming from a different layer (thick dotted ray). The desired primary scattered component (thin solid ray) is the second arrival in $G^-(x, x_2)$.

et al. (2015) note that the number of reflections undergone by an event in $G(x_2, x_1)$ (its scattering order) is equal to the sum of the number of reflections undergone by its constitutive components $G(x, x_1)$ and $G(x, x_2)$. They conclude that one component of primaries (scattering order = 1) must be a direct wave (scattering order = 0) and one component must be a first-order scattering event (Figure 1). They use that property to synthesize only multiple reflections by convolving components consisting of purely scattered waves (i.e., events with scattering order ≥ 1); this choice results in synthesis of events whose minimum wavepath scattering order is two. The results are adaptively subtracted from the measured reflection data to reveal the primaries. In this paper, we outline a related approach to predict primaries directly.

Primaries are constructed by convolving downgoing direct waves and upgoing first-order scattered waves. Following the standard decomposition of Green's functions into direct and scattered waves (e.g., $G(x, x') = G_D(x, x') + G_S(x, x')$, where $G_D(x, x')$ represents the component of $G(x, x')$ that does not undergo any reflection), direct waves are uniquely defined for any source-receiver pairs as $G_D^+(x, x_1)$ or $G_D^+(x, x_2)$. In contrast, upgoing Green's functions G_S^- comprise many first-order scattering events (in addition to multiples). This is illustrated in Figure 1a, which discriminates the construction of two different primaries. The filled circles indicate points at which direct waves are pieced together with the first-arriving events of scattered upgoing Green's functions on surface S. The unfilled circle indicates a point at which this does not apply: For that point, the associated primary reflection $G_S^-(x, x_2)$ is not the first scattered arrival. The latter case is more clearly explained in Figure 1b in which we focus on the construction associated with the unfilled circle in Figure 1a. Here, the construction associated with a primary in $G(x_2, x_1)$ (the thick solid black ray) is shown to involve the downgoing direct wave $G_D^+(x, x_1)$ (dashed black ray) and a singly scattered upgoing component of $G^-(x, x_2)$ (thin solid black ray). The latter has a larger traveltime than the first arrival of the upgoing Green's function $G^-(x, x_2)$ (dotted black ray). Thus, for arbitrary boundaries

S, the components associated with primaries do not necessarily involve direct waves and the first-arriving events of upgoing Green's functions (this is especially the case when large offsets and layers with varying velocity are considered). Finally, note that whenever multiply scattered waves in either G^- or G^+ are convolved with any event in G^+ or G^-, respectively, only the multiples are synthesized.

In Figure 2, different partial boundaries (comprising only either horizontal or vertical lines) are used to construct primaries. The filled circles and solid rays indicate points at which direct waves and the first-arriving events of upgoing Green's functions are pieced together at a stationary point to construct the corresponding primary. The unfilled circles and dashed rays indicate points at which direct waves and later, singly scattered arriving events of upgoing Green's functions are pieced together at a stationary point to construct the corresponding primary.

This shows that for a 1D medium and any x_1 and x_2 pair, if only first-arriving upgoing waves are included, then a single horizontal surface S always results in the synthesis of a single primary event (Figure 2a–2c). In contrast, a vertical portion of S may result in zero, one, or several events (Figure 2d and 2e).

Figure 3a and 3b shows the locations of a single stationary point corresponding to a primary event when different boundaries (S^u and S^d) are taken into account. The white and black squares indicate points x_α, x_β, where either the integrand $G^+(x, x_1)G^-(x, x_2)$ or $G^+(x, x_2)G^-(x, x_1)$ is stationary, respectively. Figure 3a and 3b shows that a single stationary point is sufficient to synthesize the sought primary. In Figure 3a and 3b, up- and downward pointing arrows represent normal vectors at stationary points x_α and x_β; note that for boundaries S^u and S^d, these normal vectors are antiparallel at x_α and x_β. However, if we consider a single boundary containing x_α and x_β (e.g., S^t in Figure 3c), we observe that the normals at x_α and x_β are parallel. Because each single stationary point x_α and x_β would construct the sought primary with antiparallel normals (Figure 3a and 3b), we conclude that their contributions in equations 1 and 2
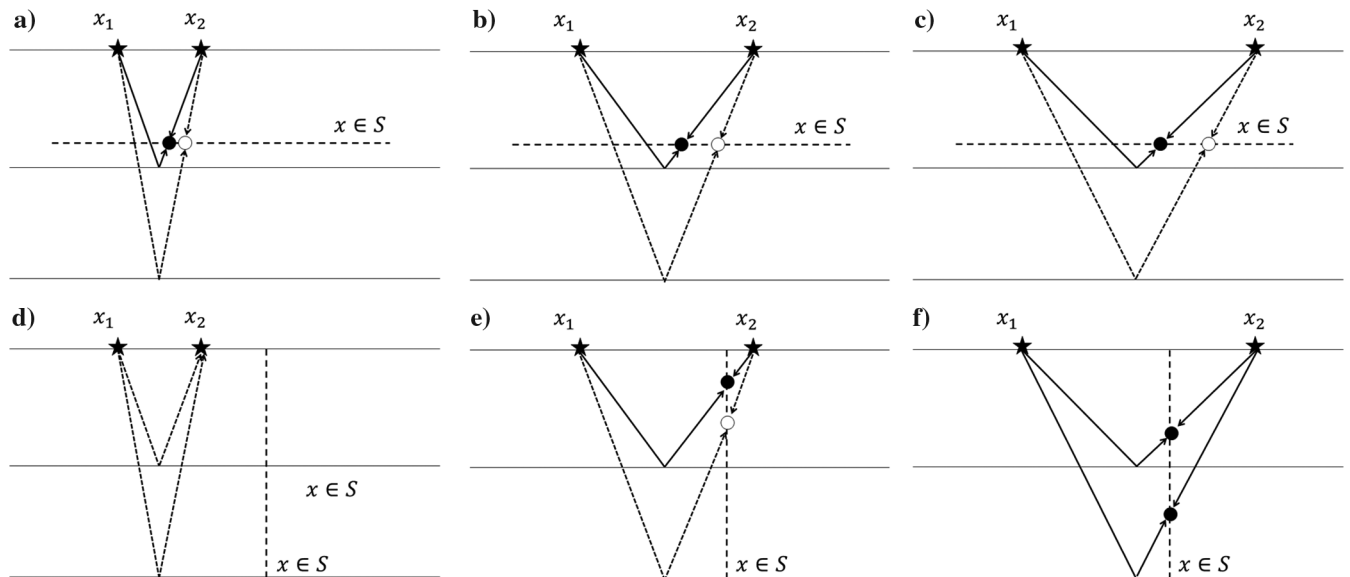

Figure 2. (a-f) Similar to Figure 1 but for limited portions of boundary S and different positions x_2. The solid rays indicate events involving direct waves and the first-arriving events of $G^-(x, x_1)$ that are therefore reconstructed by equation 3a–3c. The dashed rays indicate constructions that do not involve the first-arriving events of $G^-(x, x_1)$ that are therefore not reconstructed by equation 3a–3c.

must sum destructively when parallel normals are used (because changing the normal direction is here equivalent to multiplying the result by -1): For S^t in Figure 3c, the primary is in fact also synthesized by stationary point x_γ.

Keeping in mind the above observations and the limitations concerning performance of the method for different boundaries summarized in Figure 2, if we assume that the first-arriving energy of any upgoing Green's function $G^-(x_1, x)$ is associated with a singly scattered event, then we can reconstruct primaries by combining such events with direct waves. More precisely, we postulate that primaries, and primaries only, are reconstructed when first-arriving upgoing events are convolved with direct downgoing Green's functions. We therefore propose the following approximate representations for primaries:

$$G_P(x_2, x_1) \approx \sum_i \int_{S_i} \frac{2j\omega}{c(x)\rho(x)} \{G_F^-(x, x_2)G_D^+(x, x_1)\} dS_i, \tag{3a}$$

$$G_P(x_2, x_1) \approx \sum_i \int_{S_i} \frac{2j\omega}{c(x)\rho(x)} \{G_D^+(x, x_2)G_F^-(x, x_1)\} dS_i, \tag{3b}$$

$$G_P(x_2, x_1) \approx \sum_i \int_{S_i} \frac{2j\omega}{c(x)\rho(x)} \{G_F^-(x, x_2)G_D^+(x, x_1) + G_D^+(x, x_2)G_F^-(x, x_1)\} dS_i, \tag{3c}$$

where G_P is the Green's function's primary arrivals, G_D^+ is the direct downgoing wave, G_F^- is the first-arriving events of upgoing components of Green's functions that are created (in our examples) using Marchenko redatuming, and S_i is a partial boundary ($i = 1, 2, \ldots$). Note that equations 3a–3c correspond to the geometries depicted in Figure 3a–3c, respectively. Similar to the multiple prediction method of Meles et al. (2015), we use multiple horizontal truncated boundaries S_i, similar to that shown by the dashed thick horizontal line in Figure 3c. Summing results over multiple horizontal, vertically separated boundaries in equation 3c ensure that we can capture all primaries by at least one boundary. Although
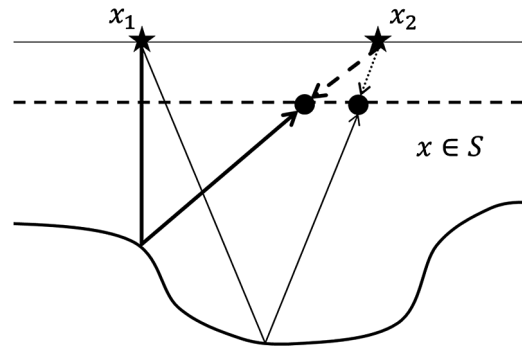

Figure 4. Complex reflector producing several primary reflections (thick and thin rays). The proposed method will synthesize each event that can be obtained as a convolution of direct and the first-arriving events of the upgoing Green's function at a stationary point along the integration boundary. Here, both events are reconstructed by different stationary points (circles) on the same boundary S.
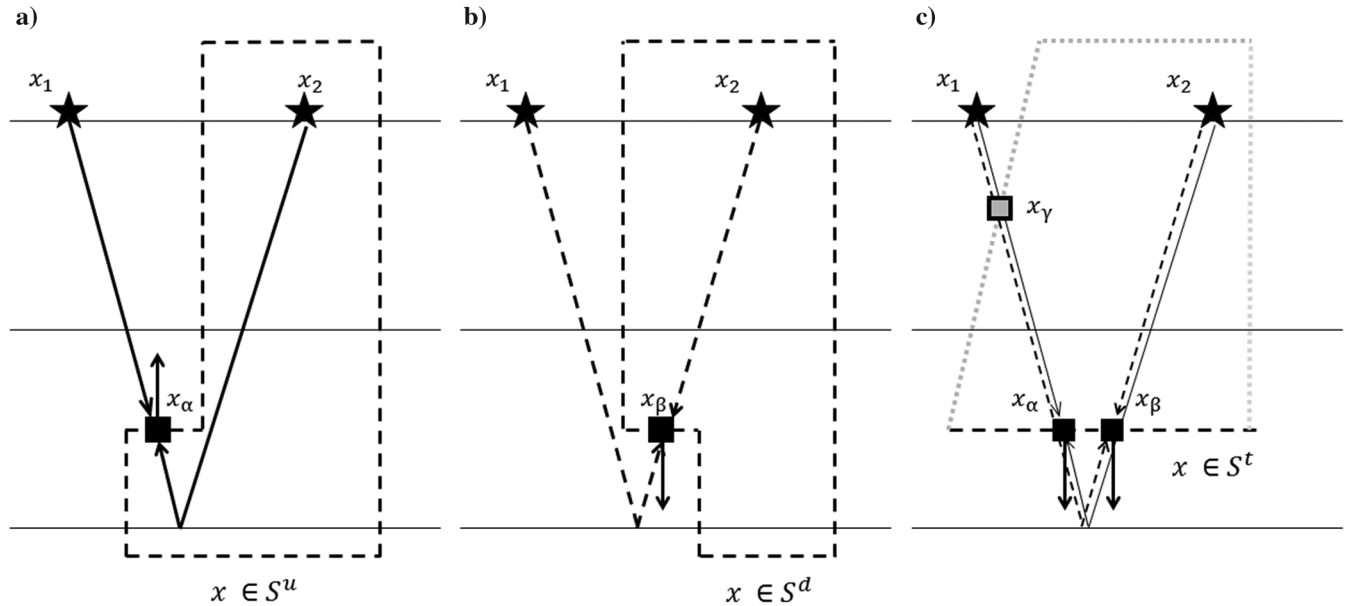

Figure 3. (a and b) The black squares indicate stationary points x_α and x_β associated with an identical primary event when different boundaries (S^u and S^d) are considered. Short arrows represent antipatallel normals at x_α and x_β, respectively. The black squares indicate points in which either the integrand $G^+(x, x_1)G^-(x, x_2)$ or $G^+(x, x_2)G^-(x, x_1)$ is stationary at x_α and x_β, respectively. (c) Mutual cancelation of stationary point contributions occurs in this case due to parallel normals at x_α and x_β. The gray square indicates an additional stationary point at x_γ whose contribution results in the depicted primary.

complex subsurface structural geometries may invalidate the above postulate, we expect it to be valid for many realistic media.

Equations 3a–3c differ crucially from the representation theorems in equations 1 and 2: Either $G_D^+(x, x_1)G_F^-(x, x_2)$ or $G_D^+(x, x_2)$ $G_F^-(x, x_1)$ only (equations 3a and 3b) or their sum (equation 3c) is integrated. These equations are consistent with our observation above regarding constructions involving only one stationary point (Figure 3a and 3b) and destructive summation due to the parallel normal along truncated horizontal boundaries (Figure 3c). Due to the latter issue, the second term in the integrand in equation 3c has the opposite sign compared with that in equation 1 or 2, which avoids the two terms mutually canceling out in the case of Figure 3c.

Equations 3a–3c result in the desired primaries provided that the stationary points of the corresponding integrands are located along the boundaries used. Note that the integrand in equation 3c is

stationary whenever either of those in equation 3a or 3b is. The distribution of stationary points of the integrands in equations 3a and 3b is a priori unknown, so boundaries must usually be chosen with a degree of arbitrariness. Such boundaries may therefore contain the stationary points of equation 3a but not those of equation 3b, or vice versa, and consequently, these equations may produce slightly different results on truncated boundaries. To maximize the probability of producing all primaries, we need to include as many stationary points as possible (i.e., those of equations 3a and 3b). Therefore, herein we apply equation 3c, even if this may result in incorrect amplitudes (as stationary points of only equation 3a or 3b, or of both may be located on each boundary used).

Several first-order reflections may be associated with a single more complex reflector (e.g., for synclinal geometries as in Figure 4), and Marchenko redatuming will correctly reproduce them
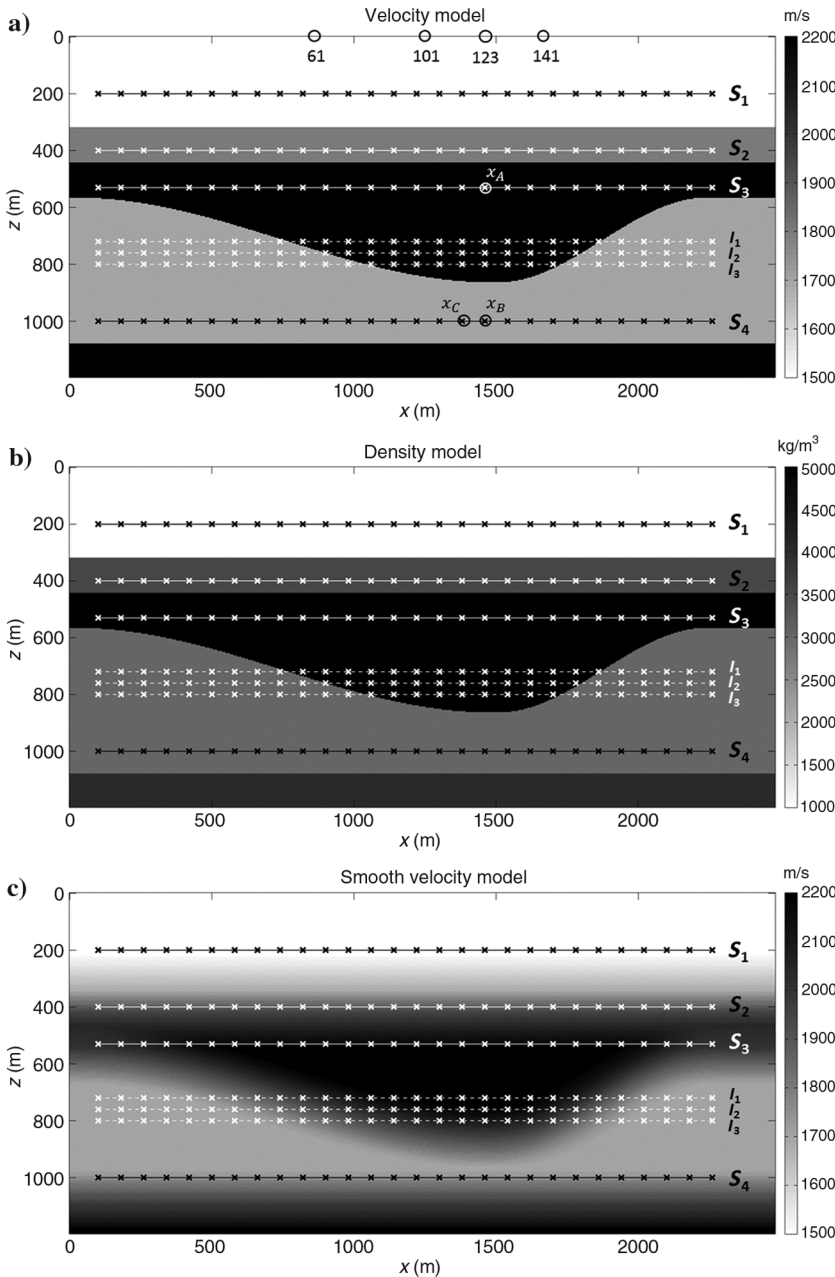

Figure 5. (a) Velocity and (b) density models used to compute the reflection data. (c) Smooth velocity model used to compute direct waves. S_1 to S_4 and I_1 to I_3 represent surfaces used for integration in equation 3c. Locations of sources 61, 101, 123, and 141 and subsurface points x_A, x_B, and x_C are shown in (a).

all (in the case that sufficient coverage is provided for each event). Equation 3c will synthesize the various primaries as long as each constituent ray can be represented as a convolution of direct and first-arriving events at different stationary points along the integration boundary (see Figure 4).

The above primary prediction method is based on representation theorems, and in principle they could estimate the exact phases and amplitudes of primaries. However, inaccuracies in Marchenko Green's functions or in the implementation of equation 3a–3c may affect the results. For example, equation 3a–3c requires knowledge of velocity $c(x)$ and density $\rho(x)$ along integration boundaries S_i. These quantities are rarely known exactly in practical situations, and therefore in our numerical experiments, we use the values in the smooth reference model for $c(x)$ and $\rho(x)$ when performing integration along boundaries S_i. However, provided $c(x)$ and $\rho(x)$ vary smoothly other than at reflectors, the use of incorrect velocity and density would usually provide accurate kinematics and only affect the amplitudes of the predicted primaries. The amplitudes could be corrected by direct comparison with the recorded data. Finally, note that each boundary S_i may generate only one or a subset of all primaries (Figure 2): Thus, by varying S_i within equation 3a–3c, we also obtain spatial information about which interfaces generate each primary.

We therefore propose the following algorithm to estimate primaries only:

1) Choose a horizontal boundary S_i in the subsurface. Locate virtual receivers at regularly sampled locations x along S_i, and use Marchenko redatuming to compute the corresponding upgoing Green's function $G^-(x, x_p)$, where source locations x_p span the surface array.
2) Mute events occurring before the direct waves in the upgoing Green's functions $G^-(x, x_p)$ to remove possible Marchenko artifacts (Thorbecke et al., 2013).
3) Pick the first-arriving event in the muted upgoing Green's function $G^-_M(x, x_p)$ to produce $G^-_F(x, x_p)$.
4) Apply equation 3c to predict primaries $G_P(x_j, x_k)$ for all x_j, x_k in the surface array.
5) Repeat steps 1–4 using S_i located at different depths to predict different primaries, and then sum the results as specified in equation 3c.

NUMERICAL EXAMPLE

We test the algorithm using a 2D varying density-velocity synclinal model (Figure 5). We compute synthetic surface seismic data with a finite-difference time-domain modeling code and a Ricker source wavelet with central frequency 20 Hz, using absorbing boundaries on all sides (thus assuming that surface-related multiples

Figure 6. (a and d) Upgoing Green's functions at virtual receivers x_A and x_B in Figure 5a, respectively, provided by Marchenko redatuming. The solid black lines indicate the kinematics of the associated direct waves, whereas the black arrows indicate artifacts. (b and e) Gathers muted before the direct wave showing reduced artifacts. (c and f) The first-arriving scattered events picked (windowed) from (b and e).
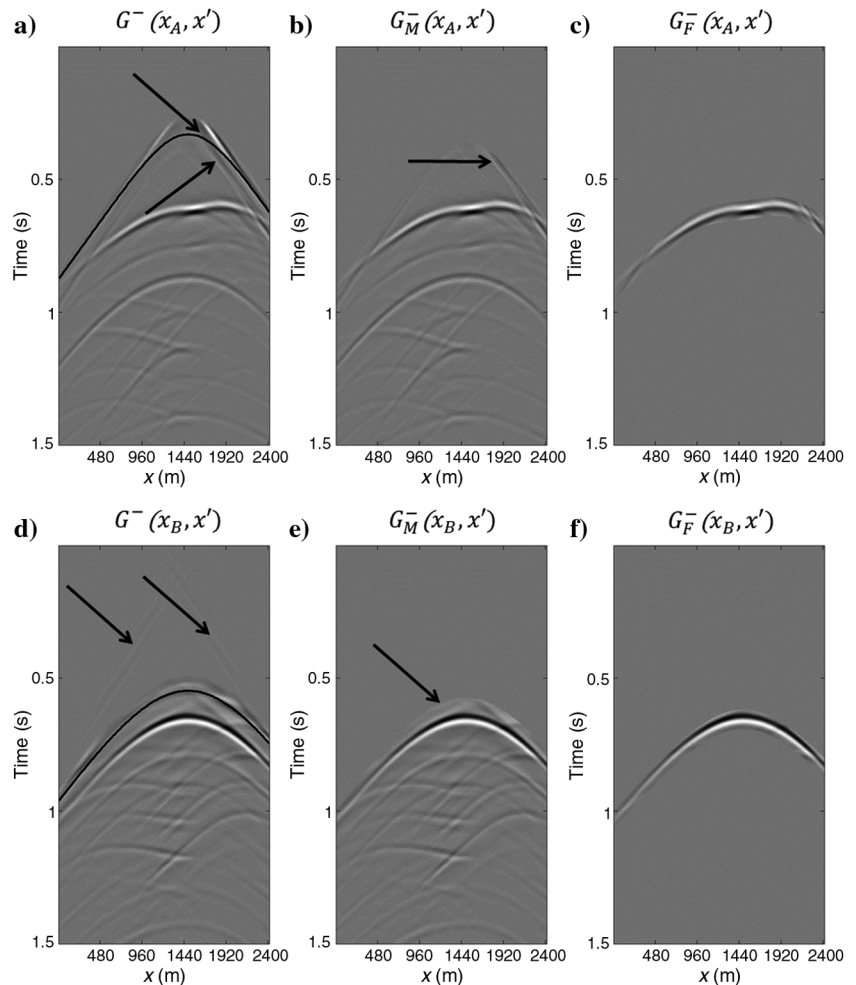
have been removed from the recorded data), between 201 colocated sources and receivers equally spaced along the surface of the model shown in Figure 5, with intersource spacing of 12 m.

Partial boundaries consist of horizontal lines S_1 to S_4 in Figure 5. Upgoing Green's functions $G^-(x, x_p)$ are estimated at a set of 121 points x along each boundary using Marchenko redatuming. We estimate direct waves $G_D^+(x, x_q)$ using a smooth velocity model (Figure 5c). The first-arriving events of upgoing Green's functions are then picked automatically and windowed.

For subsurface points x_A and x_B in Figure 5a, and x' spanning the surface sources, we discuss the picking process in more detail. The presence of refractions in the data and the inaccuracy of the modeled direct waves that are used in Marchenko redatuming result in artifacts (indicated by arrows in Figure 6) contaminating the upgoing components of the estimated Green's functions $G^-(x_{A,B}, x')$ (Thorbecke et al., 2013). To simplify the picking procedure and avoid artifacts in the estimation of primaries, we mute upgoing Green's functions so that we do not consider any energy occurring

before the corresponding direct waves $G_D^+(x_{A,B}, x')$ (Figure 6b and 6e), whose kinematics are indicated by the solid black lines in Figure 6a and 6d. We then pick the first-arriving events $G_F^-(x_{A,B}, x')$ in the muted gathers $G_M^-(x_{A,B}, x')$ by simple windowing (Figure 6c and 6f). Despite inaccuracies in these wavefields and the consequent errors in picking, primaries were relatively well reconstructed through application of equation 3c, with only small, low-amplitude artifacts (Figure 7). Note that the triplication of the primary associated with the synclinal interface, indicated by the red arrows in Figure 7, is synthesized correctly (see Figure 4).

We then apply reverse time migration (RTM; Plessix, 2006) to the observed data and the estimated primaries using the smoothed reference velocity model (Figure 5c), and the resulting images are shown in Figure 8. Linear migration of internal multiples results in many multiple-related artifacts contaminating the conventional image (as indicated by red arrows in Figure 8a). The RTM of the primaries alone provides a much cleaner image. Minor artifacts below the first reflector (as indicated by the red arrow) are due to imperfect picking
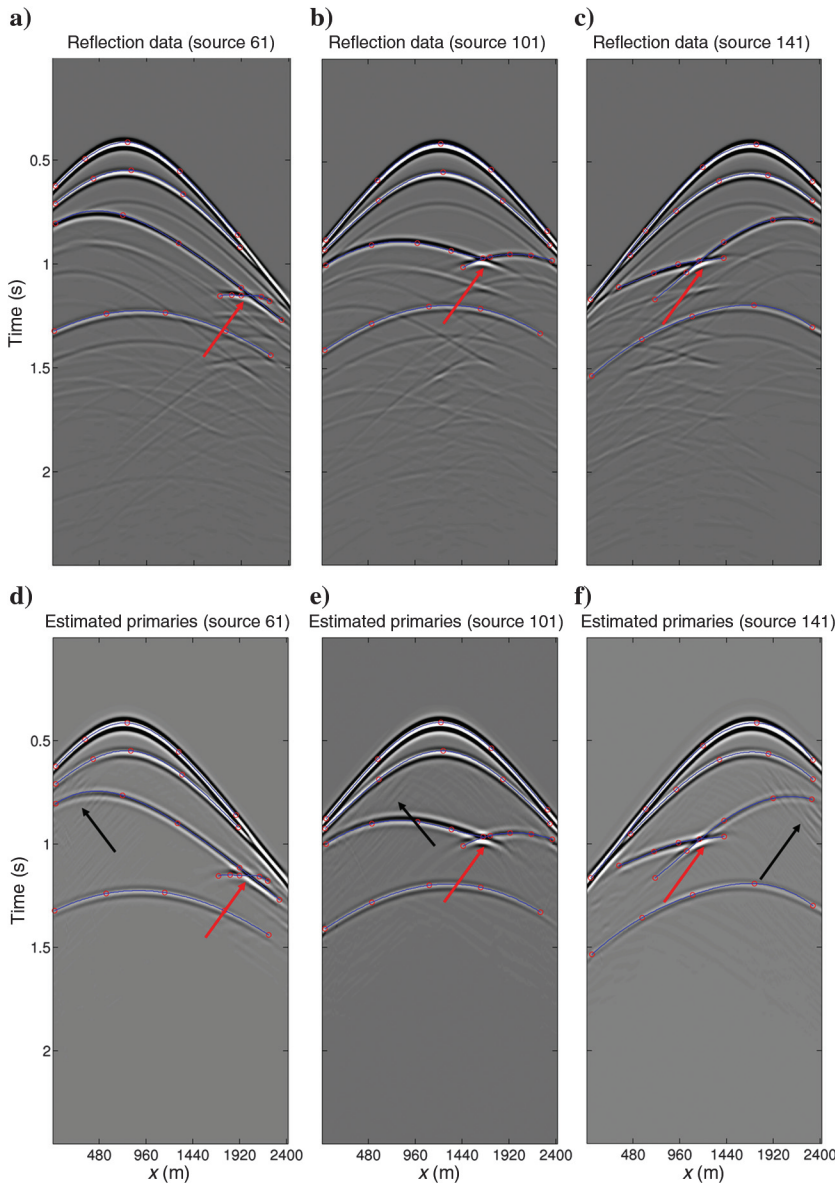

Figure 7. (a) The observed reflection data for source 61 and (d) the estimated primaries. The red arrows indicate two correctly synthesized events associated with a triplication from the same reflector (see Figure 4). Each predicted primary corresponds to an actual primary reflection indicated by the blue curves in (a and d). Low-amplitude artifacts contaminating gathers (d, e, and f) (black arrows) are due to inaccuracies in the picking process (see Figure 6b and 6c). (b and e) and (c and f): As for (a and d) but for source 101 and 141, respectively. Source locations are shown in Figure 5a.

of first-arriving events in G^-. Amplitude reduction in lateral portions of the image (left and right sides in Figure 8b) is due to inaccuracies in the Marchenko estimates caused by poor illumination of virtual receivers located in the leftmost and rightmost portions of the model.

DISCUSSION

We have presented a new method to synthesize primaries based on Marchenko redatuming and convolutional interferometry. The method requires reflection data for a set of collocated surface sources
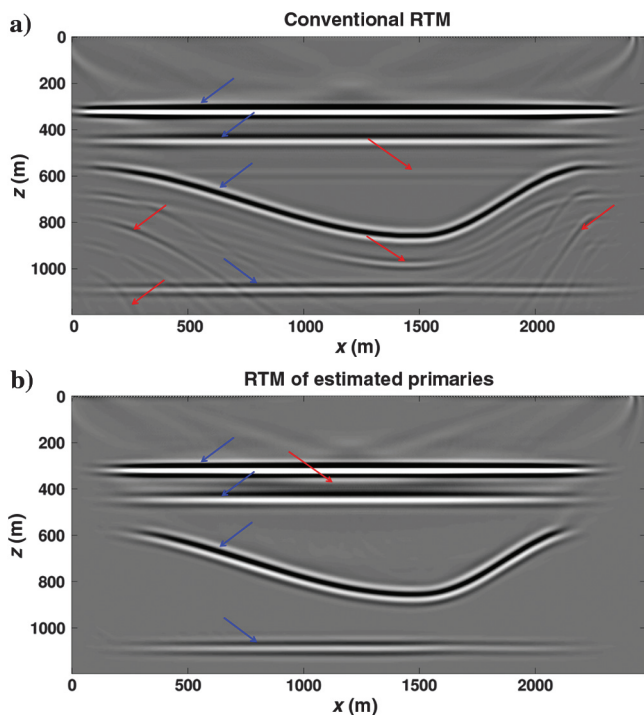

Figure 8. (a) The RTM image obtained by migrating the recorded data (primaries and internal multiples). The blue and red arrows indicate true reflectors and internal-multiple related artifacts, respectively. (b) The RTM image obtained by migrating the primaries predicted by equation 3c. The blue and red arrows indicate true reflectors and picking-related artifacts, respectively. Note that both images have saturated grayscales at 25% of their maximum amplitude to highlight weaker multiple-related artifacts.
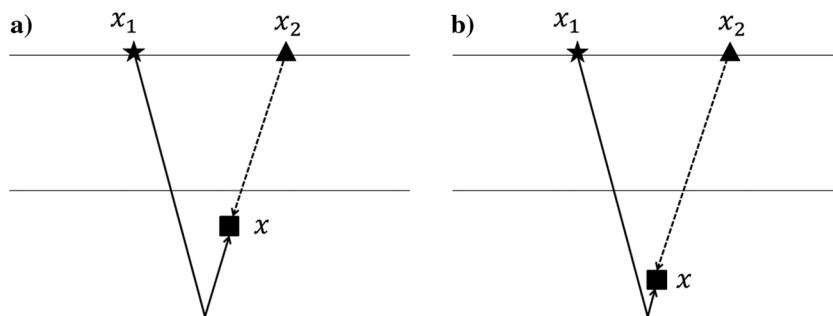

Figure 9. (a) The square indicates the virtual receiver location, when the exact velocity model is used for Marchenko redatuming. The solid and dashed rays represent up- and downgoing Green's function components, respectively. (b) Same as (a), but using an erroneous velocity model effectively shifts the position of the virtual receiver created by Marchenko redatuming.

and receivers and estimates of the direct wave from the surface to each virtual receiver in the subsurface, which may be challenging for complex models. Nevertheless, we showed that primaries are predicted reasonably well despite using a highly smoothed velocity model for direct wave estimation (Figure 5c). This is because Marchenko redatuming is a time-domain method and small errors in timing of direct waves result in time shifts of opposite sign in up- and downgoing components. Because these components are convolved in our method (equation 3a–3c) and hence their phases (traveltimes) are added, such errors cancel and have little effect on the results (see the cartoon in Figure 9). This is better illustrated in Figure 10, in which Marchenko gathers obtained with different velocity models are compared. Gathers (a) and (c) show down- and upgoing Green's functions retrieved using the correct velocity model for point $x_A (x = 1480 \text{ m}, z = 530 \text{ m})$ and x' spanning the surface sources in Figure 5a. Gathers (b) and (d) show down- and upgoing Green's functions that were obtained using a velocity model perturbed by 10%. For the zero-offset trace collected above x_A, the down- and upgoing components at the stationary point in the convolutional gathers are indicated by arrows in Figure 10. Note that when using the wrong velocity model, exactly opposite shifts in time affect down- and upgoing gathers. Their convolution is therefore almost unaffected by the relative errors and the primary is synthesized correctly. This is shown in Figure 11 in which the primary associated with the synclinal interface is properly reconstructed despite the use of the wrong velocity model in the Marchenko redatuming step.

The need to convolve the first-arriving events of upgoing Green's functions and downgoing direct waves requires the use of Marchenko redatuming to estimate these components, rather than using standard wavefield extrapolation methods as are used in RTM, for example. The latter methods usually produce upgoing gathers contaminated by nonphysical, coherent events associated with internal multiples. Some of these artifacts may occur before the first-arriving event of the true upgoing Green's function (see Figure 12). They would then be picked and jeopardize the performance of the primary method because convolving these events with direct waves would reproduce internal multiples.

Automating the picking process required by our method can be challenging because small artifacts in the upgoing Green's function gathers might be picked erroneously (Thorbecke et al., 2013). By contrast, the demultiple method of Meles et al. (2015), which is also based on Marchenko redatuming and convolutional interferometry, does not require any picking, but its performance is limited by errors in (adaptive) multiple subtraction procedures, similar to all other multiple removal algorithms published to-date (Guitton and Verschuur, 2004). This limitation is entirely removed by the primaries synthesis algorithm proposed here.

The choice of the integration boundaries S_i plays a key role in our algorithm. To reproduce all of the primaries with correct relative amplitudes, each S_i should lie above each reflector. If several boundaries are chosen within a homogeneous stratum, the same primary will be predicted multiple times. Stacking over different boundaries (as given in equation 3c) would then result in errors in the relative amplitudes of the different primaries, similar to relative amplitudes of multiples in the method of Meles et al. (2015).
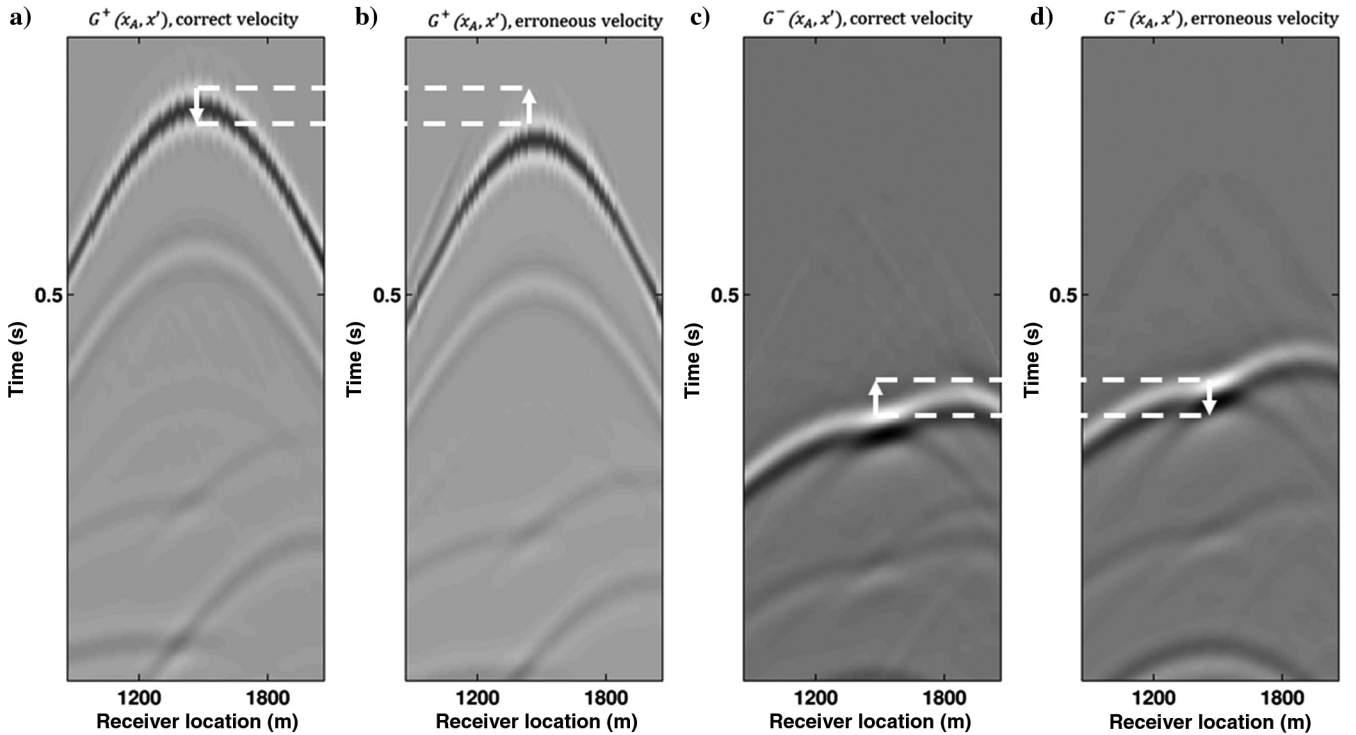
Figure 10. (a and b) Downgoing and (c and d) upgoing Green's function estimates as provided by Marchenko redatuming using exact (a and c) and erroneous (b and d) velocity models. Opposite time shifts apply to down- and upgoing gathers when erroneous velocity models (in this case 10% too fast) are used (white arrows).
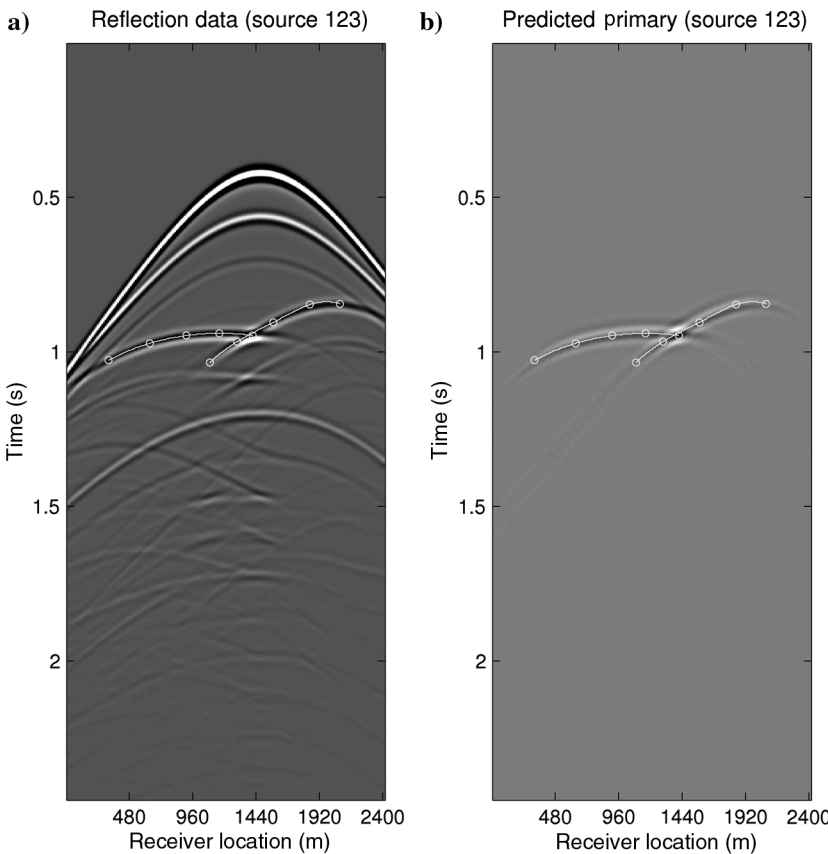

Figure 11. (a) The observed reflection data for source 123. (b) The estimated primaries using a single convolutional line S_3 and a velocity model perturbed by 10%. The predicted primary corresponds to an actual primary reflection (indicated by the white curves in [a and b]).

In our synthetic test, for simplicity we used horizontal integration boundaries, but this is not a requirement of the method (arbitrarily shaped boundaries can be used). We also considered the ideal case of single integration boundaries between each pair of reflectors. This choice not only provides good relative amplitudes of primaries, but it also allows easier implementation of the method because the first-arriving upgoing events are all associated with the same interface. However, in practical applications, erroneous or approximate prior estimates of the subsurface structure may result in integration boundaries that intersect interfaces (Meles et al., 2015). In Figure 13, we consider a similar situation by using integration boundaries I_1 to I_3 (Figure 5) and source number 101. When boundaries which intersect interfaces are used, primaries (black curves) are only partially reconstructed (Figure 13a–13c). Note that in Figure 13a–13c, two primaries are partially synthesized for complementary receiver subsets, and the white arrows indicate artifacts in the primary gathers. These artifacts are due to nonstationary contributions of the integrand at points at which boundaries intersect an interface. This is better illustrated in Figure 14, where, with the aid of a cartoon, we investigate in

more detail the artifacts labeled A and B in Figure 13b, corresponding to source 101 and receiver 93 (dashed line in Figure 13b). These artifacts are not stationary with respect to the location of the boundary lines, and hence they are eventually attenuated by summing over multiple boundaries (black arrows in Figure 13d).

Complex subsurface structures may require many integration boundaries to avoid the problems discussed above. In standard applications, a fairly dense grid of redatuming points throughout the medium (similar to that provided locally by I_1 to I_3 in Figure 5) could be used. As a consequence, the proposed algorithm would become rather expensive, and its total costs might approach that of redatuming via multidimensional deconvolution (MDD) to all subsurface points. However, in contrast to MDD, our method does not require any inversion, and furthermore, it produces multiple-free data at the ground acquisition surface. This is an important difference with respect to MDD redatuming because our method can be used not only to perform RTM but also to provide primaries-only data for other linearized processing steps that require linearized data (e.g., velocity analysis).

Figure 12. (a) $G^-(x_C, x')$ estimate as provided by Marchenko redatuming. The black arrow indicates the first-arriving event. (b) Standard extrapolation gather at x_C derived by RTM. The white arrows indicate internal-multiple related artifacts occurring before the first-arriving physical energy (black arrow).
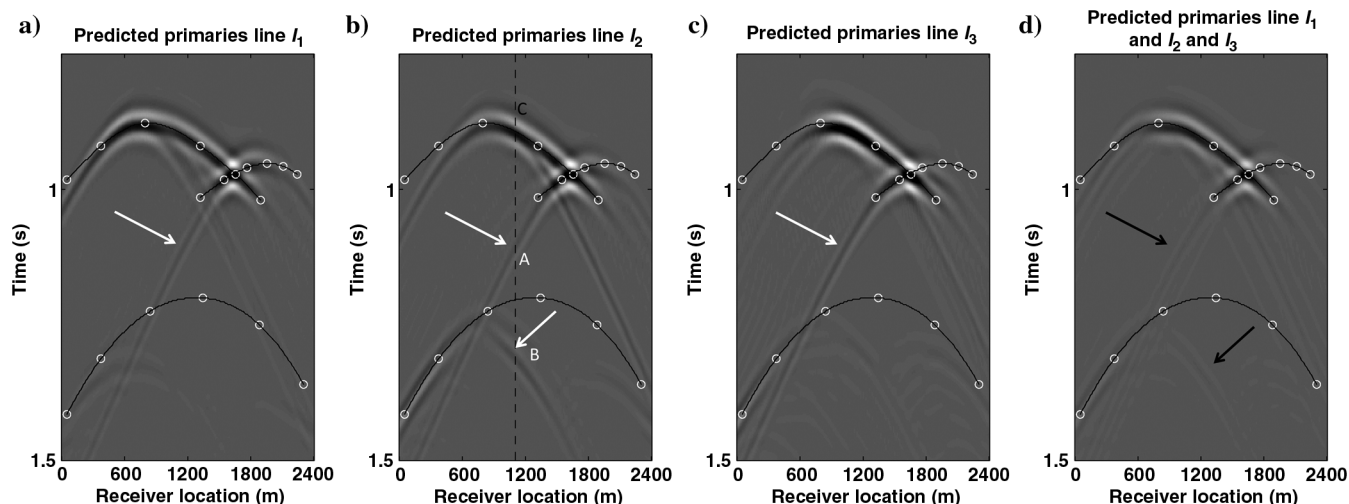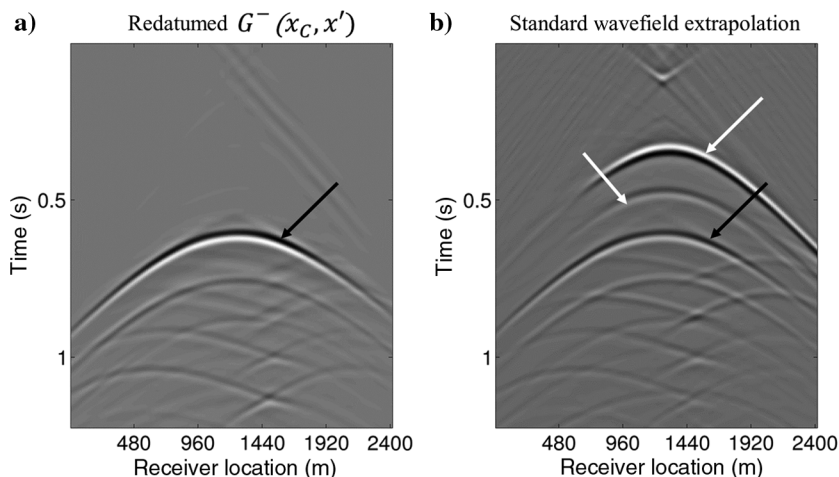

a) Redatumed $G^-(x_C, x')$

b) Standard wavefield extrapolation

a) Predicted primaries line I_1
b) Predicted primaries line I_2
c) Predicted primaries line I_3
d) Predicted primaries line I_1 and I_2 and I_3

Figure 13. (a) The estimated primaries corresponding to source 101 and integration boundary I_1. Exact primaries are indicated by black curves. The white arrows indicate artifacts. (b and c): as for (a) but when boundaries I_2 and I_3 are used, respectively. (d) Summation of gathers (a-c). The black arrows indicate residual low amplitude artifacts. In (b), the dashed line indicates receiver 93, labels A and B denote two distinct artifacts, and C corresponds to the true primary associated with the syncline.

Note that there are other subsurface structural geometries that may invalidate our postulate that primaries are synthesized by the convolution of a direct wave with the first-arriving event of the upgoing wavefield. In Figure 15, we show two further challenging scenarios in which the convolution of the first-arriving upgoing fields and direct waves (a) does not construct a primary event or (b) produces a refracted wave. Clearly, when these types of refracted waves occur, the method is not expected to give perfect results. Note also that Marchenko redatuming is based on up/down decomposition, and the presence of horizontally propagating waves may affect its performances.

The cost of one iteration of Marchenko redatuming, which we may consider as the unit cost U for this methodology, is equivalent to that of a multidimensional convolution for each source-receiver pair at the acquisition level. A total number of $n_r \times n_s$ convolutions are then required, where n_r and n_s are the number of receivers and sources, respectively. As in standard Marchenko applications, sources and receivers are collocated, and the unit cost involves n_r^2 convolutions. Note that the number of sources and receivers can increase dramatically when moving from 2D to 3D applications, and so does the unit cost. Several iterations (n_i) are required before convergence is achieved (in our synthetic tests, we used $n_i = 6$ iterations). In 2D and 3D integration, boundaries are lines and surfaces, respectively. Each integration boundary may comprise of up to hundreds (in 2D) or thousands (in 3D) of virtual receiver locations (n_v), depending on the size of the model, to conform to the Nyquist criterion. Finally, several or many boundaries (n_b) may be needed for complex subsurface geometries. In total, the overall cost of the method is given by: $n_i \times n_v \times n_b \times U$. Optimization of the computational cost could be achieved by minimizing/optimizing the number of boundaries to be used and by involving other primary events in the Marchenko redatumed upgoing Green's functions in addition to the first-arriving waves. A more detailed discussion about the computation costs in Marchenko redatuming can be found in Behura et al. (2014).

Finally, note that Marchenko redatuming was used in this manuscript because it provides separated wavefields at subsurface receiver locations. However, any method and acquisition configuration that allow up-/downgoing wavefields to be estimated in the subsurface could be used within the algorithm discussed here. Any improvement in either quality or efficiency of those methods compared with Marchenko redatuming would then be expected to be inherited by our method.
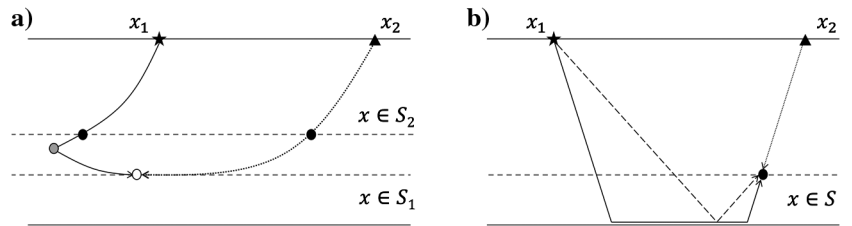

Figure 15. Complex geometries and refractions that invalidate our assumption concerning the synthesis of primary reflections via convolutional interferometry of the first-arriving upgoing fields and direct waves. In (a), a primary event associated with a diffractor (gray dot) is seen to involve the convolution of horizontally propagating direct and scattered fields at the stationary point (white circle) on S_1 due to the bending of rays. Note that the assumption would be valid if a different boundary like S_2 had been used (black circles are the corresponding stationary points). (b) A refracted event is constructed by convolving the first-arriving upgoing Green's functions ($G^-(x, x_1)$, solid line) and downgoing direct wave ($G_D^+(x, x_2)$, solid line). In this case, the reflected wave (dashed line) may have larger traveltime to the stationary point (black circle) than the refracted arrival.
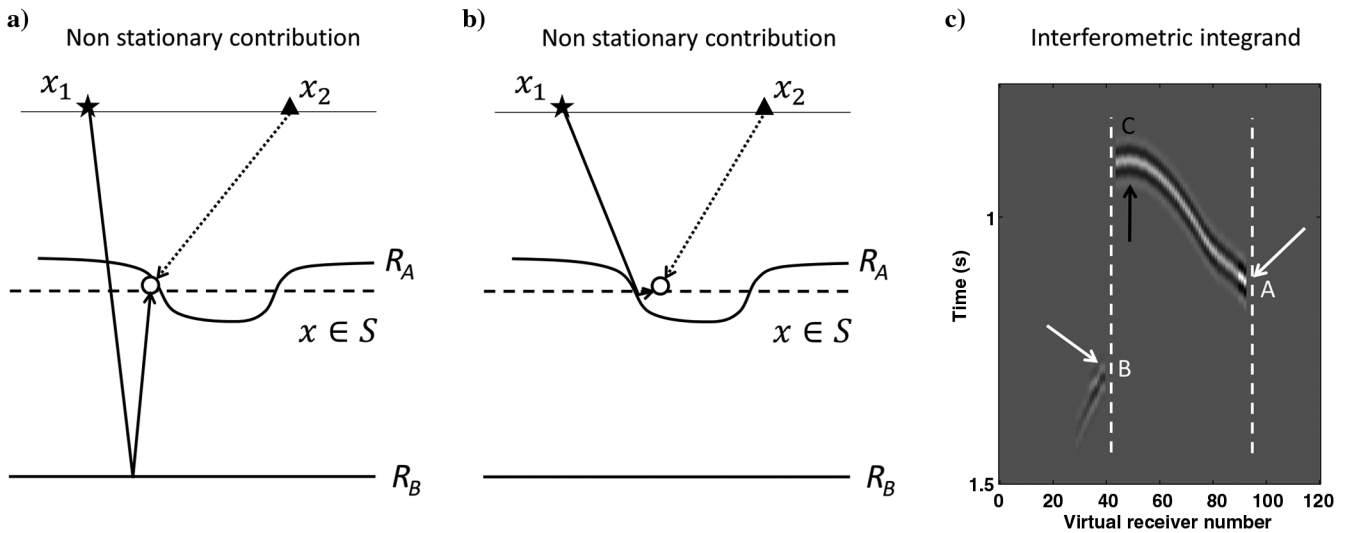

Figure 14. (a) The white circle indicates a nonstationary point of $G_D^+(x, x_2) G_F^-(x, x_1)$ with $G_F^-(x, x_1)$ being generated by reflector R_B. As x passes through the interface R_A from the left of the figure, $G_F^-(x, x_1)$ is generated by reflector R_A as shown in (b), and cancelation of the nonstationary contribution in (a) does not take place (and for different geometries similar arguments would apply also to $G_D^+(x, x_1) G_F^-(x, x_2)$). (c) Integrand of equation 3c for source 101, receiver 93, and integration line I_2. Artifacts A and B in Figure 13b are due to nonstationary events (A and B in [c]) associated with discontinuities in the integrand. For simple models, we expect $G_D^+(x, x_{1,2})$ to be continuous functions of x. Therefore, discontinuities of the integrand depend on discontinuities in $G_F^-(x, x_{1,2})$. Finally, C indicates the stationary contribution of the integrand that actually produces the true primary event in Figure 13b.

CONCLUSIONS

We presented a new method to predict primary reflections based on Marchenko redatuming and convolutional interferometry. The method was demonstrated on acoustic data and proved to be stable with respect to inaccuracies in the redatumed Green's functions. The synthesized primaries were used to produce images free of multiple-related artifacts via linear RTM. For simplicity, the method has been tested on a surface-related multiple free data set recorded for collocated sources and receivers. Extension to data sets collected in standard acquisition setups and including ghosts and surface-related multiples will be the topic of future research. Applications connected to other methods such as full-waveform inversion and velocity analysis will also be investigated.

ACKNOWLEDGMENTS

REFERENCES

Behura, J., and F. Forghani, 2012, A practical approach to prediction of internal multiples and ghosts: 82nd Annual International Meeting, SEG, Expanded Abstracts, doi: 10.1190/segam2012-1269.1.

Behura, J., K. Wapenaar, and R. Snieder, 2014, Autofocus imaging: Image reconstruction based on inverse scattering theory: Geophysics, **79**, no. 3, A19–A26, doi: 10.1190/geo2013-0398.1.

Berkhout, A. J., and D. J. Verschuur, 1997, Estimation of multiple scattering by iterative inversion, Part I: Theoretical consideration: Geophysics, **62**, 1586–1595, doi: 10.1190/1.1444261.

Broggini, F., R. Snieder, and K. Wapenaar, 2012, Focusing the wavefield inside an unknown 1D medium — Beyond seismic interferometry: Geophysics, **77**, no. 5, A25–A28, doi: 10.1190/geo2012-0060.1.

Broggini, F., R. Snieder, and K. Wapenaar, 2014, Data-driven wave field focusing and imaging with multidimensional deconvolution: Numerical examples for reflection data with internal multiples: Geophysics, **79**, no. 3, WA107–WA115, doi: 10.1190/geo2013-0307.1.

Campillo, M., and A. Paul, 2003, Long-range correlations in the diffuse seismic coda: Science, **299**, 547–549.

da Costa Filho, C. A., M. Ravasi, and A. Curtis, 2015, Elastic P and S wave autofocus imaging with primaries and internal multiples: Geophysics, **80**, no. 5, S187–S202, doi: 10.1190/geo2014-0512.1.

da Costa Filho, C. A., M. Ravasi, A. Curtis, and G. A. Meles, 2014, Elastodynamic Green's function retrieval through single-sided Marchenko inverse scattering: Physical Review E, **90**, 063201, doi: 10.1103/PhysRevE.90.063201.

Dragoset, B., E. Verschuur, I. Moore, and R. Bisley, 2010, A perspective on 3D surface-related multiple elimination: Geophysics, **75**, no. 5, 75A245–75A261, doi: 10.1190/1.3475413.

Gray, S., J. Etgen, J. Dellinger, and D. Whitmore, 2001, Seismic migration problems and solutions: Geophysics, **66**, 1622–1640, doi: 10.1190/1.1487107.

Guitton, A., and D. J. Verschuur, 2004, Adaptive subtraction of multiples using the L1-norm: Geophysical Prospecting, **52**, 27–38, doi: 10.1046/j.1365-2478.2004.00401.x.

Hung, B., and M. Wang, 2012, Internal demultiple methodology without identifying the multiple generators: 82nd Annual International Meeting, SEG, Expanded Abstracts, doi: 10.1190/segam2012-0549.1.

Jakubowicz, H., 1998, Wave equation prediction and removal of interbed-multiples: 68th Annual International Meeting, SEG, Expanded Abstracts, 1527–1530.

Malcolm, A. E., B. Ursin, and V. Maarten, 2009, Seismic imaging and illumination with internal multiples: Geophysical Journal International, **176**, 847–864

Meles, G., K. Löer, M. Ravasi, A. Curtis, and C. A. da Costa Filho, 2015, Internal multiple prediction and removal using Marchenko autofocusing and seismic interferometry: Geophysics, **80**, no. 1, A7–A11, doi: 10.1190/geo2014-0408.1.

Plessix, R., 2006, A review of the adjoint-state method for computing the gradient of a functional with geophysical applications: Geophysical Journal International, **167**, 495–503, doi: 10.1111/gji.2006.167.issue-2.

Ravasi, M., I. Vasconcelos, A. Kritski, A. Curtis, C. A. da Costa Filho, and G. A. Meles, 2016, Target-oriented Marchenko imaging of a North Sea field: Geophysical Journal International, **205**, 99–104, doi: 10.1093/gji/ggv528.

Snieder, R., K. Wapenaar, and K. Larner, 2006, Spurious multiples in seismic interferometry of primaries: Geophysics, **71**, no. 4, SI111–SI124, doi: 10.1190/1.2211507.

Thorbecke, J., J. van der Neut, and K. Wapenaar, 2013, Green's function retrieval with Marchenko equations: A sensitivity analysis: 83rd Annual International Meeting, SEG, Expanded Abstracts, 3888–3893.

Van der Neut, J., K. Wapenaar, J. Thorbecke, E. Slob, and I. Vasconcelos, 2015, An illustration of adaptive Marchenko imaging: The Leading Edge, **34**, 818–822, doi: 10.1190/tle34070818.1.

van Manen, D.-J., A. Curtis, and J. O. A. Robertsson, 2006, Interferometric modeling of wave propagation in inhomogeneous elastic media using time reversal and reciprocity: Geophysics, **71**, no. 4, SI47–SI60, doi: 10.1190/1.2213218.

van Manen, D.-J., J. O. A. Robertsson, and A. Curtis, 2005, Modeling of wave propagation in inhomogeneous media: Physical Review Letters, **94**, 164301-1–164301-4, doi: 10.1103/PhysRevLett.94.164301.

Virieux, J., and S. Operto, 2009, An overview of full-waveform inversion in exploration geophysics: Geophysics, **74**, WCC1–WCC26.

Wang, M., B. Hung, and K. Xin, 2012, Application of inverse scattering series method for internal multiple attenuation: A case study: ASEG, Extended Abstracts, doi: 10.1071/ASEG2012ab148.

Wapenaar, K., 2004, Retrieving the elastodynamic Green's function of an arbitrary inhomogeneous medium by cross correlation: Physical Review Letters, **93**, 254301-1–254301-4, doi: 10.1103/PhysRevLett.93.254301.

Wapenaar, K., 2014, Single-sided Marchenko focusing of compressional and shear waves: Physical Review E, **90**, 063202, doi: 10.1103/PhysRevE.90.063202.

Wapenaar, K., and A. Berkhout, 1989, Elastic wave field extrapolation: Redatuming of single- and multi-component seismic data: Elsevier Science Publishing Company Inc.

Wapenaar, K., F. Broggini, and R. Snieder, 2012, Creating a virtual source inside a medium from reflection data: Heuristic derivation and stationary-phase analysis: Geophysical Journal International, **190**, 1020–1024, doi: 10.1111/j.1365-246X.2012.05551.x.

Wapenaar, K., and J. Fokkema, 2006, Green's function representations for seismic interferometry: Geophysics, **71**, no. 4, SI33–SI46, doi: 10.1190/1.2213955.

Wapenaar, K., J. Thorbecke, J. van der Neut, F. Broggini, E. Slob, and R. Snieder, 2014a, Green's function retrieval from reflection data, in absence of a receiver at the virtual source position: Journal of the Acoustical Society of America, **135**, 2847–2861, doi: 10.1121/1.4869083.

Wapenaar, K., J. Thorbecke, J. van der Neut, F. Broggini, E. Slob, and R. Snieder, 2014b, Marchenko imaging: Geophysics, **79**, no. 3, WA39–WA57, doi: 10.1190/geo2013-0302.1.

Wapenaar, K., J. van der Neut, E. Ruigrok, D. Draganov, J. Hunziker, E. Slob, J. Thorbecke, and R. Snieder, 2011, Seismic interferometry by crosscorrelation and by multidimensional deconvolution: A systematic comparison: Geophysical Journal International, **185**, 1335–1364, doi: 10.1111/j.1365-246X.2011.05007.x.

Weglein, A., F. Araújo, P. Carvalho, R. Stolt, K. Matson, R. Coates, D. Corrigan, D. Foster, S. Shaw, and H. Zhang, 2003, Inverse scattering series and seismic exploration: Inverse Problems, **19**, R27–R83, doi: 10.1088/0266-5611/19/6/R01.

Weglein, A., F. A. Gasparotto, P. M. Carvalho, and R. H. Stolt, 1997, An inverse-scattering series method for attenuating multiples in seismic reflection data: Geophysics, **62**, 1975–1989, doi: 10.1190/1.1444298.

Yilmaz, O., 2001, Seismic data analysis: Processing, inversion and interpretation of seismic data: SEG.

Zhu, J., L. Lines, and S. Gray, 1998, Smiles and frowns in migration/velocity analysis: Geophysics, **63**, 1200–1209, doi: 10.1190/1.1444420.